4

Feedback Signals

… in which three feedback signals are selected for control of active power and it is shown that the geographical variation of phase angle mode observability agrees with that of active power mode controllability.

Feedback signals carry information while control signals carry energy. As information is so much simpler to handle than energy, the freedom to choose feedback signals for a damping system is in general considerable: a variable that is not physically measurable may be estimated or synthesized from one or more other available quantities. A variable that cannot be conveniently measured at the desirable location can be remotely measured and telemetered via some sort of communication link.

Three signals are proposed for control of active power:

- local bus frequency;
- frequency of the closest machine;
- estimated mode frequency.

The two first signals will be used in several dampers at different network locations in Chapters 7 and 8, while the third one will only be used for damping of a local mode with one damper as described in Chapters 5 and 6. All three signals have been used for damping with PSS (see paper and discussion of [Larsen and Swann 1981]). To a certain extent they describe the velocity of the machine rotors, which is natural, as it is their motion that should be damped.

General requirements on feedback signals for damping are discussed in Section 4.1, and expressions for their mode observability are given in Section 4.2. The geographical variation of mode observability for bus frequency is computed for the test systems in Section 4.3. It is analytically shown that for each mode the optimum place to measure bus frequency at is where active power has the best effect on damping. This makes local feedback preferable, which is advantageous in many aspects. The meaning of the closest machine is outlined in Section 4.4 while estimated mode frequency is treated in Section 4.5. Section 4.6 concludes the results.

4.1 Feedback Signal Selection

A feedback signal for control of a certain actuator to damp a power system should fulfil a number of requirements:

- realistic sensor and signal processing needs;
- limited demands on communication bandwidth and delay;
- adequate phase and amplitude of the mode observability;
- characteristics insensitive to change of operating point or network topology.

Whereas the first three issues are fairly straightforward to check, the last one is difficult but very important. In general, a damping system is aimed at a set of modes that may have different phase characteristics. The fact that the frequencies of these modes may lie very close to each other, and can shift as the operating point or the network state changes makes the design of a suitable phase compensation network difficult. Insensitivity to this change in system parameters is often referred to as *robustness*.

Design of robust controllers typically requires extensive numerical investigations. These may use repeated linearization [Jones 1996] of an ordinary model, or methods that can handle uncertainty such as H_∞ or μ design techniques [Maciejowski 1989]. Instead of using these numerical alternatives the control laws suggested in the following will be based on structural knowledge about the physical behaviour of the system. This method is less straightforward, but yields a controller whose robustness is related to the validity of a physical law rather than to numerical properties of the system. The required structural knowledge is obtained from the mechanical equivalents of Section 2.4. These are well prepared as their force input correspond to controlled active power input, which is the type of actuator chosen in Chapter 3.

4.2 Computing Mode Observability

To evaluate a feedback signal, its ability to detect a certain mode is of primary interest. As a mode has a geographical extent and the measurement of the signal can be done at different places, the geographical variation of *mode observability* should be studied. From this the suitability of the signal *and* an appropriate location to measure it can be concluded.

Mode observability is closely related to the right eigenvectors of a system. This gives the same restrictions on valid comparisons that applied to mode controllability: Only the mode controllability of variables that describe the

same physical quantity and have the same scaling can be compared. Measures for different modes can not be compared to each other.

A right eigenvector and its eigenvalue contain all information about how all the elements of the state vector move during a mode motion. As stated by (2.9), the eigenvalue gives the frequency and damping, while the eigenvector elements determine the amplitude and phase shift of the more or less damped sinusoidal motion of each state. In a DAE model both dynamic states, algebraic variables and outputs are feedback signal candidates. Fig. 2.3 indicates that the expressions for their mode observability are different. The mode motion of the dynamic states x_d are given directly by the right eigenvectors. These are found as columns in the right modal matrix of the ODE system,

$$\Phi$$

or equivalently by the dynamic part of the right DAE system eigenvectors obtained from (2.12),

$$\Phi_{dae,d}$$

The influence of the mode motion on the algebraic states x_a in a DAE model is,

$$-A_{22}^{-1}A_{21}\Phi \tag{4.1}$$

while the coupling from mode to explicit outputs is governed by,

$$\left(C_1 - C_2 A_{22}^{-1} A_{21}\right)\Phi \tag{4.2}$$

where the parenthesized expression is equal to C_{ode}. The output matrices C_1 and C_2 may be formed for the observability analysis instead of including the outputs in the model. This procedure limits the model complexity, while still offering the requested information. As an example, phase angle at a network bus does not appear as a variable in the DAE model exported by the simulation program EUROSTAG. Instead it can be determined from the bus voltage elements as,

$$\Delta\theta = \frac{1}{V^2}\begin{bmatrix} -v_I & v_R \end{bmatrix}\begin{bmatrix} \Delta v_R \\ \Delta v_I \end{bmatrix} \tag{4.3}$$

where V is bus voltage magnitude, v_R+jv_I is the linearization point and Δ denotes deviation from it.

4.3 Local Bus Frequency

The generic damping component in a spring-mass model is a viscous damper. When moving one of its ends relative to the other, the damper develops a counteracting force proportional to the velocity of the motion. Introducing a damper as in Fig. 4.1, would intuitively damp an oscillating motion of the masses as the swing energy is dissipated in the damper.

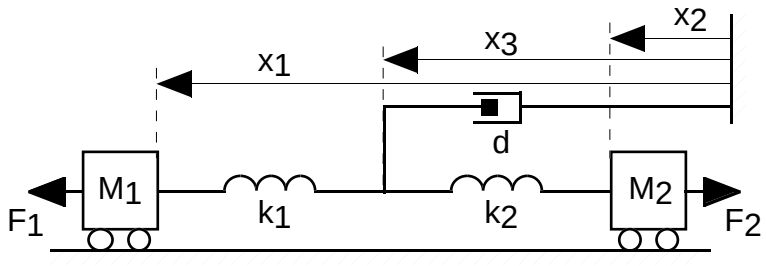

Fig. 4.1 Viscous damper introduced in the spring-mass model of an inter-area mode.

The arrangement gives a force F_3 that is d_3 times the velocity of its point of attack. In a power system this is equivalent to active power proportional to the local bus frequency deviation. This control law has been proposed for damping controllers in HVDC links by for example [Smed 1993]. A difference here is that it will be employed simultaneously at different locations in the network.

Bus frequency is obtained by filtering measurements of the phase angle. Taking the time derivative of a sinusoidal signal gives a phase shift of 90° and adds a factor equal to the angular velocity. The mode observability for the bus frequency thus differs from that of the phase angle by a factor equal to j times the eigenfrequency of the mode, which is the imaginary part of the corresponding eigenvalue. For more details on techniques to determine bus frequency, see [Phadke et al 1983].

Mode Observability for Analytical Models

The mode observability of x_3 in the spring-mass model (2.29) of an inter-area mode can be obtained from the right eigenvector in (2.31) by using (4.1),

$$-A_{22}^{-1}A_{21}\Phi_1 = \frac{1}{k_1+k_2}\begin{bmatrix}0 & 0 & k_1 & k_2\end{bmatrix}\begin{bmatrix}\frac{\lambda_1}{M_1} & \frac{-\lambda_1}{M_2} & \frac{1}{M_1} & \frac{-1}{M_2}\end{bmatrix}^T = \frac{\frac{k_1}{M_1}-\frac{k_2}{M_2}}{k_1+k_2} \tag{4.4}$$

Clearly, the observability is large close to the masses, and zero at a point between them, which could be called a *swing node*. The mode observability in x_3 and the mode controllability of the force F_3 as given by (3.5) thus exhibit exactly the same dependence on k_1 and k_2.

The mode observability of x_2 in the pendulum in Fig. 2.12 is,

$$-A_{22}^{-1}A_{21}\Phi_1 = \frac{l_2}{l_1+l_2}$$

Performing the same computations for the spring-mass model of (2.33) and the power system of (2.20) yield the following expressions for the mode observability of x_2

$$\frac{k_1}{k_1+k_2}$$

and of θ,

$$-K_{\theta\theta}^{-1}K_{\theta\delta} = -K_{\delta\theta}^{T}K_{\theta\theta}^{-1}$$

For all three systems, the mode observability of the phase angle or its equivalent increases as the measurement point is moved closer to the swinging mass. The geographical variation of this mode observability is thus the same as that of the mode controllability measures of active power or force derived in Section 3.3. This property constitutes the type of highly desirable structural information mentioned in Section 4.1. It can be proven that the agreement applies for a multi-machine power system with a general network.

Depart from the description of (2.22) and omit the Δ notations. Eliminating θ gives the ODE formulation of the system,

$$\begin{cases}\dot{x} = Ax + Bu\\ y = Cx + Du\end{cases}$$

with

$$x = \begin{bmatrix} \omega \\ \delta \end{bmatrix};\ u = P_{load}\ ;\ y = \theta;$$

$$A = \begin{bmatrix} 0 & M^{-1}K \\ I & 0 \end{bmatrix};\quad B = \begin{bmatrix} M^{-1}K_{\delta\theta}K_{\theta\theta}^{-1} \\ 0 \end{bmatrix};$$

$$C = \begin{bmatrix} 0 & -K_{\theta\theta}^{-1}K_{\theta\delta} \end{bmatrix};D = \begin{bmatrix} K_{\theta\theta}^{-1} \end{bmatrix}$$

where

$$K = K_{\delta\delta} - K_{\delta\theta}K_{\theta\theta}^{-1}K_{\theta\delta}$$

Due to the total lack of damping, the eigenvalues of this system are purely imaginary. Use the state transformation as in the proof of eigenvector similarity in [Eliasson 1990],

$$\tilde{x} = \tilde{M}^{1/2}x = \begin{bmatrix} M^{1/2} & 0 \\ 0 & M^{1/2} \end{bmatrix}x;$$

This yields the new system matrices,

$$\tilde{A} = \begin{bmatrix} 0 & M^{-1/2}KM^{-1/2} \\ I & 0 \end{bmatrix};\quad \tilde{B} = \begin{bmatrix} M^{-1/2}K_{\delta\theta}K_{\theta\theta}^{-1} \\ 0 \end{bmatrix};$$

$$\tilde{C} = \begin{bmatrix} 0 & -K_{\theta\theta}^{-1}K_{\theta\delta}M^{-1/2} \end{bmatrix};D = \begin{bmatrix} K_{\theta\theta}^{-1} \end{bmatrix}$$

Partition the right and left eigenvectors Φ_i and Ψ_i of the eigenvalue λ_i into angular velocity and angle parts,

$$\Phi_i = \begin{bmatrix} \Phi_{i\omega} \\ \Phi_{i\delta} \end{bmatrix};\ \Psi_i = \begin{bmatrix} \Psi_{i\omega} & \Psi_{i\delta} \end{bmatrix}$$

Entering this into (2.7) gives,

$$\begin{aligned} \Phi_{i\omega} &= \lambda_i\Phi_{i\delta} \\ 0 &= \left(M^{-1/2}KM^{-1/2} + \lambda_i^2 I\right)\Phi_{i\delta} \end{aligned} \tag{4.5}$$

Assume that $\Phi_{i\delta}$ is real. This is possible since the parenthesized expression is real. Similar expressions for the left eigenvectors are based on (2.8),

$$\begin{aligned} \Psi_{i\delta} &= \lambda_i\Psi_{i\omega} \\ 0 &= \Psi_{i\omega}\left(M^{-1/2}KM^{-1/2} + \lambda_i^2 I\right) \end{aligned} \tag{4.6}$$

As all matrices within the parenthesis of (4.5) and (4.6) are symmetric it can be concluded that,

$$\Psi_{i\omega} = \rho_i \xi_i \Phi_{i\delta}^T \tag{4.7}$$

where ρ_i is a positive real scalar and ξ_i is a complex scalar that are chosen so that $\Psi_i \Phi_i = 1$ for all nonzero eigenvalues. Here it is sufficient to determine ξ_i so that the argument of $\Psi_i \Phi_i$ is zero. Using (4.5)-(4.7) gives,

$$\begin{aligned}\begin{bmatrix}\Psi_{i\omega} & \Psi_{i\delta}\end{bmatrix}\begin{bmatrix}\Phi_{i\omega} \\ \Phi_{i\delta}\end{bmatrix} &= \begin{bmatrix}\Psi_{i\omega} & \lambda_i \Psi_{i\omega}\end{bmatrix}\begin{bmatrix}\lambda_i \Phi_{i\delta} \\ \Phi_{i\delta}\end{bmatrix} \\ &= \rho_i \xi_i \begin{bmatrix}\Phi_{i\delta}^T & \lambda_i \Phi_{i\delta}^T\end{bmatrix}\begin{bmatrix}\lambda_i \Phi_{i\delta} \\ \Phi_{i\delta}\end{bmatrix} \\ &= 2\rho_i \xi_i \lambda_i \Phi_{i\delta}^T \Phi_{i\delta}\end{aligned}$$

It is evident that ξ_i should have the same argument as the inverse of λ_i and therefore $\xi_i = \lambda_i^{-1}$ will be used in the following. Both left and right eigenvectors can now be expressed in terms of $\Phi_{i\delta}$, λ_i and ρ_i.

The observability of mode i in the phase angles θ at the load buses is then given by,

$$\tilde{C}\Phi_i = -K_{\theta\theta}^{-1} K_{\theta\delta} M^{-1/2} \Phi_{i\delta}$$

Similarly the active power controllability of mode i at the load buses is ,

$$\Psi_i \tilde{B} = \Psi_{i\omega} M^{-1/2} K_{\delta\theta} K_{\theta\theta}^{-1} = \lambda_i^{-1} \rho_i \Phi_{i\delta}^T M^{-1/2} K_{\delta\theta} K_{\theta\theta}^{-1}$$

Taking the transpose of this and using (4.7) together with the properties of $K_{\theta\theta}$, $K_{\delta\theta}$ and $K_{\theta\delta}$ yields,

$$\left(\Psi_i \tilde{B}\right)^T = \rho_i \lambda_i^{-1} K_{\theta\theta}^{-1} K_{\theta\delta} M^{-1/2} \Phi_{i\delta} = -\rho_i \lambda_i^{-1} \tilde{C}\Phi_i \tag{4.8}$$

For each mode and at all load buses the mode controllability of active power and the mode observability of the phase angle are thus proved to be proportional. This property does not depend on the choice of coordinates, and therefore applies also to the original coordinates. It is however important to realize that the result is only guaranteed to apply as long as the used model is valid.

For each mode, the measurement signal best reflecting the mode is thus available where the actuator is most efficient. The resulting feedback is

therefore local and eliminates long distance communication with its associated problems.

Let active power injection at a bus be controlled as a gain K times the local bus frequency obtained as the time derivative of the phase angle. Taking the time derivative of a sinusoidal signal adds a phase shift of 90° and multiplies the signal by its angular frequency. For mode i the resulting control law at bus k is,

$$P_k = K\lambda_i\theta_k$$

The eigenvalue sensitivity to K is obtained by inserting (4.8) into (2.11) and including λ_i of the controller,

$$\frac{\partial\lambda_i}{\partial K} = \psi_i\tilde{B}\lambda_i\tilde{C}\Phi_i = -\rho_i\left(\tilde{C}\Phi_i\right)^T\tilde{C}\Phi_i \qquad (4.9)$$

Since ρ_i is real and positive, the sensitivity of (4.9) is real and negative. At least for small gains, active power controlled by local bus frequency will therefore add damping to *all* modes simultaneously – irrespective of where in the system such a damper is installed.

The same agreement between the magnitude of mode controllability and mode observability but for reactive power and voltage magnitude is mentioned in [Smed and Andersson 1993]. Implicitly it forms the basis for the SVC control law in [Gronquist et al 1995], where the SVC output is controlled in proportion to the time derivative of the local bus voltage magnitude. By the use of energy function analysis it is shown that this local feedback improves damping regardless of where in the system the equipment is located. The close relationship to the control law suggested above is apparent. By inserting this in the energy function used in [Gronquist et al 1995], the same beneficial effect on damping can probably be shown to apply for active power controlled by local bus frequency. If this is the case the controlled active power need not vary symmetrically around zero, but can be limited for example to zero from above or below. Such a proof, which is carried out for a local mode system in Chapter 5, would verify the assumption in Section 3.1, that temporary disconnection of a load can be used to improve damping.

Mode Observability for Numerical Models

The analytical results above are based on highly simplified power system models. Their validity in a more realistic system is therefore not evident,

but can be examined by studying the test systems with three and twenty-three machines respectively.

The three-machine model includes line resistance and generator flux dynamics. This makes analytical treatment impractical and instead the phase angle mode observability in the network is determined numerically. For the load situation in question, the imaginary part of the voltage is small and the voltage magnitude is very close to one at all buses. This simplifies (4.3) substantially so that the phase angle mode observability can be obtained directly from the Δv_I elements of the right eigenvector corresponding to the electro-mechanical modes. This is quite similar to the procedure for determining active power controllability for the same system in Section 3.3. The complex nature of the observability measure is treated in the same way: by projecting the points in the complex plane on a line obtained as a least square fit to the points of the machine angle elements. Fig. 4.2 shows the line and the complex phase angle mode observability of all network buses. As a complement, the complex values of phase angle mode observability for the load buses are given in Table 4.1.

Bus	1.3 Hz mode	1.8 Hz mode
N5	$0.152e^{-j170°}$	$0.028e^{j100°}$
N6	$0.130e^{-j169°}$	$0.095e^{j76°}$
N8	$0.332e^{-j175°}$	$0.086e^{j83°}$

Table 4.1 Complex phase angle mode observability at the load buses of the three machine system.

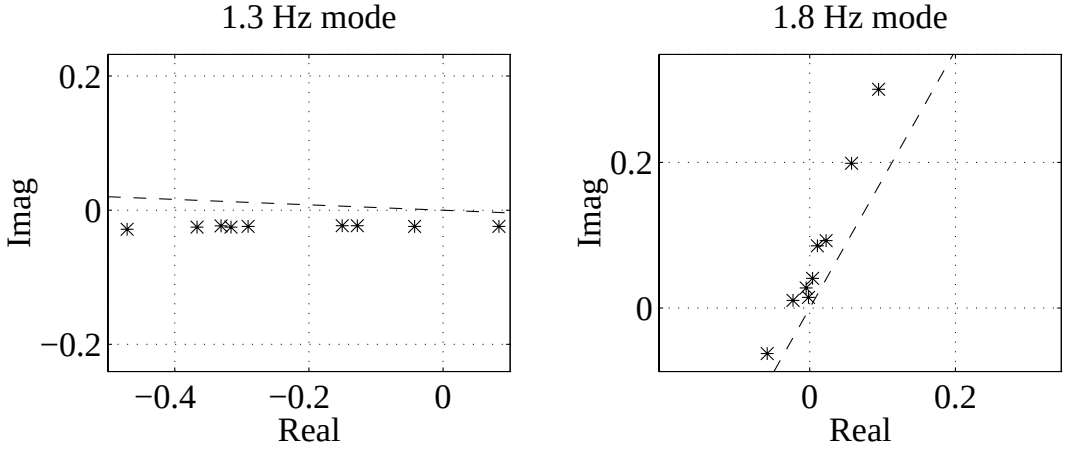

Fig. 4.2 Complex phase angle mode observability of the three machine system for the 1.3 Hz mode (left) and the 1.8 Hz mode (right) as compared to the line based on machine angle mode observability.

As the deviation from the line is small in both cases, substantial information is not lost through the projection. The geographical variation in the network of mode observability can now be illustrated using the same technique as in Fig. 3.3. Thinking in terms of bending modes of flexible mechanical structures is even more motivated here, as observability and mode shape both are extracted from the right eigenvectors. The result in Fig. 4.3 shows great agreement with the active power mode controllability in Fig. 3.3 and the interpretations are the same.

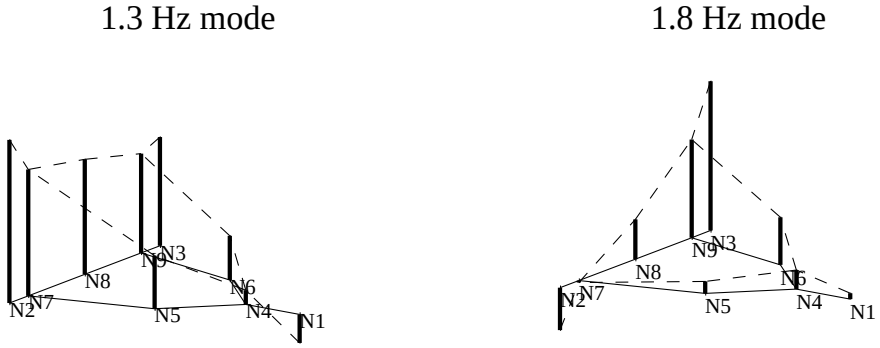

Fig. 4.3 Phase angle mode observability of the three machine system for the 1.3 Hz mode (left) and the 1.8 Hz mode (right).

The twenty-three machine system model is even less simplified than that with three machines. Important differences are damper windings, nonlinear loads and PSSs. The phase angle mode observability is obtained in much the same way as for the three machine system. Due to the high loading situation however, (4.3) needs to be employed and the resulting complex values for the load buses are given in Table 4.2. These numbers are distributed in the complex plane as in Fig. 4.4 for the selected modes in the fault case.

Bus	Mode 1	Mode 2	Mode 3
N1011	$0.027e^{j144°}$	$0.006e^{j170°}$	$0.002e^{j72°}$
N1012	$0.029e^{j145°}$	$0.008e^{j167°}$	$0.003e^{-j6°}$
N1013	$0.032e^{j148°}$	$0.009e^{j167°}$	$0.005e^{-j8°}$
N1022	$0.015e^{j132°}$	$0.017e^{-j27°}$	$0.036e^{j137°}$
N1041	$0.127e^{-j5°}$	$0.071e^{j166°}$	$0.036e^{j127°}$
N1042	$0.101e^{-j5°}$	$0.016e^{-j171°}$	$0.176e^{j139°}$
N1043	$0.097e^{-j4°}$	$0.022e^{j175°}$	$0.082e^{j138°}$
N1044	$0.058e^{-j1°}$	$0.034e^{-j27°}$	$0.125e^{j141°}$
N1045	$0.165e^{-j6°}$	$0.146e^{j164°}$	$0.050e^{-j21°}$
N2031	$0.016e^{j19°}$	$0.040e^{-j24°}$	$0.079e^{j140°}$
N2032	$0.005e^{j85°}$	$0.054e^{-j24°}$	$0.093e^{j138°}$
N4071	$0.038e^{j144°}$	$0.042e^{j158°}$	$0.057e^{-j41°}$
N4072	$0.044e^{j144°}$	$0.063e^{j158°}$	$0.091e^{-j42°}$
N41	$0.053e^{j0°}$	$0.040e^{-j24°}$	$0.076e^{j143°}$
N42	$0.041e^{-j1°}$	$0.050e^{-j24°}$	$0.137e^{j141°}$
N43	$0.048e^{j0°}$	$0.052e^{-j24°}$	$0.151e^{j141°}$
N46	$0.048e^{j0°}$	$0.057e^{-j24°}$	$0.165e^{j141°}$
N47	$0.043e^{j0°}$	$0.068e^{-j23°}$	$0.186e^{j141°}$
N51	$0.190e^{-j6°}$	$0.223e^{j163°}$	$0.099e^{-j25°}$
N61	$0.113e^{-j5°}$	$0.037e^{-j24°}$	$0.019e^{-j65°}$
N62	$0.135e^{-j6°}$	$0.038e^{-j24°}$	$0.059e^{-j50°}$
N63	$0.143e^{-j6°}$	$0.062e^{-j21°}$	$0.083e^{-j50°}$

Table 4.2 Complex phase angle mode observability at the load buses of the twenty-three machine system.

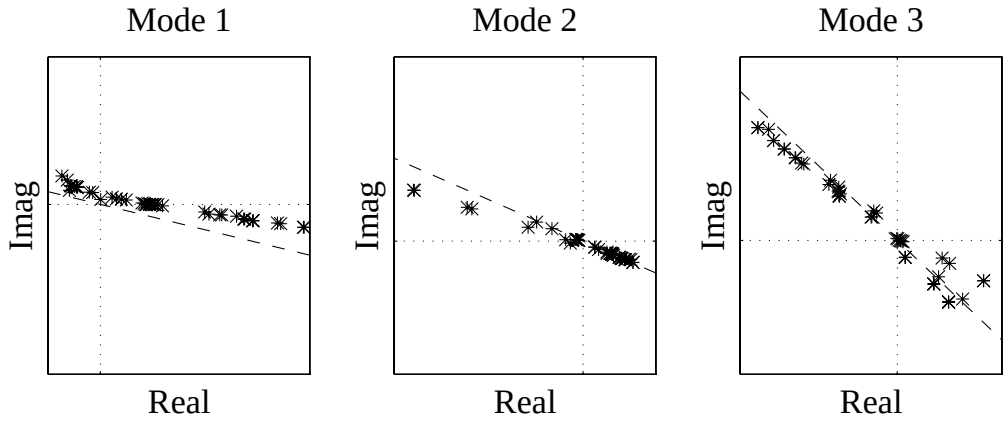

Fig. 4.4 Complex phase angle mode observability of the twenty-three machine system in the fault case for Mode 1 (left), Mode 2 (middle) and Mode 3 (right) as compared to the lines based on machine angle mode observability.

Again, the points are projected onto a line with a direction equal to the mean direction of the machine angle observability of all generators. The geographical variation can finally be visualized along with the network topology as in Fig. 4.5 for the three modes.

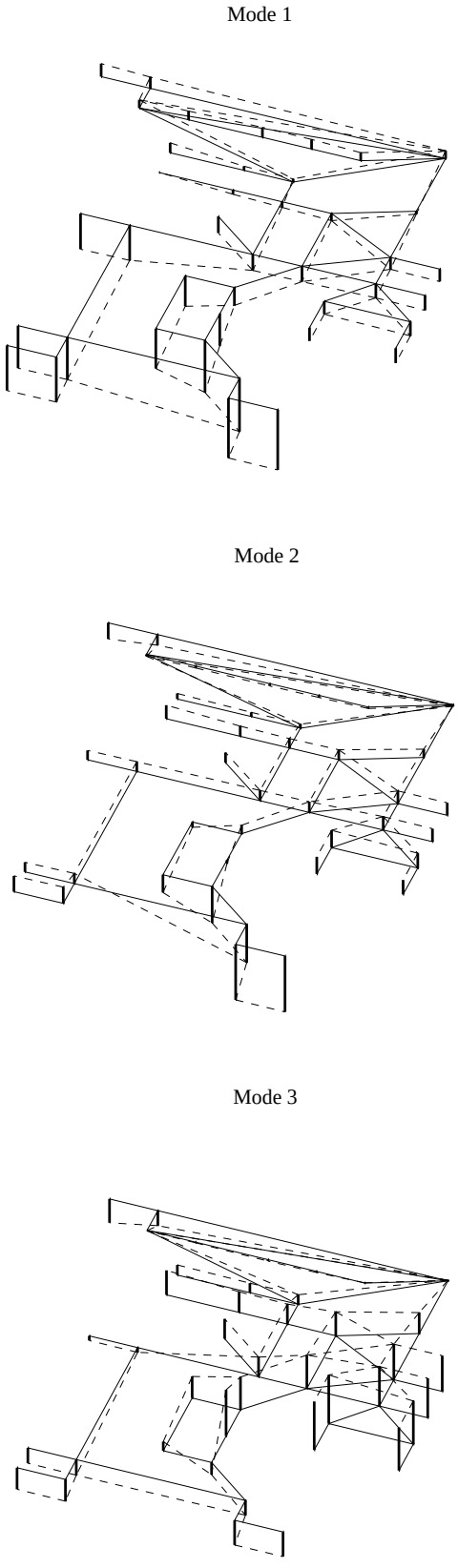

Fig. 4.5 Phase angle mode observability of the twenty-three machine system in the fault case for Mode 1 (top), Mode 2 (middle) and Mode 3 (bottom).

Fig. 4.5 is very similar to the geographical variation of the active power controllability in Fig. 3.5, and differences can be found mainly in magnitude. More importantly, the sign is different at the buses close to N4051 for Mode 3 in the fault case. A screening of all modes shows that this is the only significant exception from the rule that the geographical variation of active power mode controllability and phase angle mode observability are, if not identical, then at least very similar.

If local feedback from bus frequency to active power is introduced in the area close to bus N4051, the eigenvalue sensitivity of Mode 3 to the gain will differ from that predicted by (4.9) by 180°. Increasing the gain from zero to a small value will thus start to move the eigenvalues of Mode 3 to the right. As with all sensitivity analysis, nothing can be said about the continued locus of the eigenvalues. This is better treated with root locus analysis, which will be applied in Chapter 7.

4.4 Closest Machine Frequency

The damping system should damp the motions of the oscillating masses. Measuring their velocity is then an obvious and more direct alternative to measuring velocity at the actuator location. On the other hand these signals, corresponding to rotor angular velocity of power system generators, need to be telemetered. In a large power system measurements would have to be sent from all machines to all actuators. To keep down communication requirements, this is reduced to using only the rotor angular velocity or frequency of the closest machine. The same choice is suggested in [Stanton and Dykas 1989] and [Larsen and Hill 1993].

In the previous section it was shown that active power controlled by the bus frequency anywhere in the system shifts all eigenvalues straight into the left half plane as long as the gain is small. It seems reasonable to assume that this property applies also if the measurement point is not exactly the same as the actuator location, but sufficiently *close* to it. As shown in Section 3.3 "*close*" is related to the mass-scaled electrical distance rather than the geographical distance. For the spring-mass model damping is obtained as long as the measurement point and the actuator location are on the same *side* of the swing node. In a larger system the same condition is expressed in terms of acceptable *regions* for the different modes. If the mode controllability can be visualized by the 3D-views used in Figs 3.3 and 3.5 these may be used define the regions. For an actuator located in a region, feedback from the rotor angular velocity of any machine in that region will damp the corresponding mode. As the regions are different for different modes, the machine that lies in the same region as

the actuator for *all* modes is accepted. Practically, it may be sufficient if this is true only for the modes where the controllability of the actuator at the given location is considerable.

Although being illustrative, the described method is not very exact. An alternative is to numerically compute the eigenvalue sensitivity for different combinations of machines and actuator locations. According to (2.11) and (2.16) this is the product of active power mode controllability and machine frequency mode observability. The complex values of active power mode controllability at the load buses are given in Tables 3.1 and 3.2 for the two multi-machine test systems. The machine frequency mode observability is obtained from the angular velocity elements of the right DAE or ODE eigenvectors. The values for the three machine system are given below in Table 4.3.

Machine	1.3 Hz mode	1.8 Hz mode
H1	$2.230e^{j89°}$	$0.330e^{-j16°}$
S2	$6.583e^{-j88°}$	$3.250e^{-j32°}$
S3	$3.978e^{-j87°}$	$10.91e^{j156°}$

Table 4.3 Complex mode observability for the angular velocity of the machines in the three machine system.

Table 4.4 contains the corresponding complex numbers for all the machines in the twenty-three machine system.

Machine	Mode 1	Mode 2	Mode 3
A1042	$0.414e^{j80°}$	$0.051e^{-j72°}$	$1.609e^{-j132°}$
A1043	$0.363e^{j78°}$	$0.026e^{-j115°}$	$0.801e^{-j132°}$
A4042	$0.114e^{j74°}$	$0.441e^{j67°}$	$1.146e^{-j132°}$
A4047_1	$0.136e^{j74°}$	$0.618e^{j67°}$	$1.676e^{-j131°}$
A4047_2	$0.136e^{j74°}$	$0.618e^{j67°}$	$1.676e^{-j131°}$
A4051_1	$0.832e^{j81°}$	$1.765e^{-j110°}$	$0.901e^{j62°}$
A4051_2	$0.850e^{j80°}$	$1.836e^{-j112°}$	$0.926e^{j60°}$
A4062	$0.565e^{j81°}$	$0.408e^{j71°}$	$0.527e^{j38°}$
A4063_1	$0.621e^{j81°}$	$0.668e^{j71°}$	$0.821e^{j38°}$
A4063_2	$0.621e^{j81°}$	$0.668e^{j71°}$	$0.821e^{j38°}$
B4011	$0.113e^{-j118°}$	$0.047e^{-j98°}$	$0.029e^{j120°}$
B4012	$0.121e^{-j118°}$	$0.060e^{-j102°}$	$0.047e^{j85°}$
B4021	$0.004e^{-j64°}$	$0.216e^{j65°}$	$0.500e^{-j134°}$
B4031	$0.025e^{j62°}$	$0.256e^{j66°}$	$0.487e^{-j133°}$
B4071	$0.161e^{-j124°}$	$0.292e^{-j113°}$	$0.425e^{j48°}$
B4072	$0.187e^{-j126°}$	$0.445e^{-j114°}$	$0.681e^{j47°}$
B1012	$0.125e^{-j119°}$	$0.059e^{-j102°}$	$0.044e^{j80°}$
B1013	$0.135e^{-j119°}$	$0.065e^{-j103°}$	$0.052e^{j81°}$
B1014	$0.141e^{-j118°}$	$0.072e^{-j105°}$	$0.070e^{j76°}$
B1021	$0.140e^{-j108°}$	$0.151e^{j60°}$	$0.274e^{-j146°}$
B1022	$0.083e^{-j113°}$	$0.100e^{j63°}$	$0.202e^{-j137°}$
B2032	$0.027e^{-j82°}$	$0.373e^{j65°}$	$0.651e^{-j135°}$
C4041	$0.219e^{j90°}$	$0.301e^{j64°}$	$0.594e^{-j130°}$

Table 4.4 Complex mode observability for the angular velocity of the machines in the twenty-three machine system.

Depending on which location that is chosen for the actuator, suitable machines are chosen and the corresponding controllability and observability are multiplied to give eigenvalue sensitivity.

4.5 Estimated Mode Frequency

The ultimate feedback signal for damping a mode would be the mode coordinate itself. In principle this involves all the machine angles weighted by the right eigenvector of the mode, which in most cases is unrealistic. The (inter-area) mode involving two areas, however is structurally simple

as each machine group can be represented as a large machine with a representative machine angle as in Fig. 4.6.

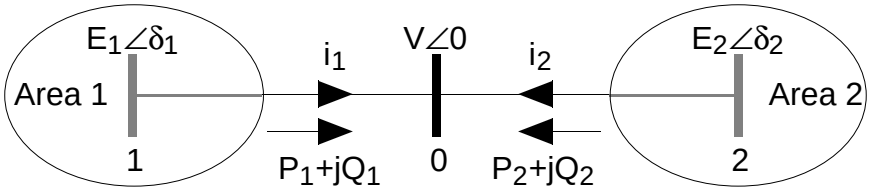

Fig. 4.6 Two area system.

The angles δ_1 and δ_2 are the mass weighted means of the individual machine angles in the two groups. The angle $\delta=\delta_1-\delta_2$ closely reflects the inter-area mode. If the two areas are connected via a set of transmission lines, δ may be synthesized from local measurements at the intermediate bus as in [Larsen et al 1995] and [Lerch et al 1991]: introduce the complex variables $\bar{i}_1$, $\bar{i}_2$, $\overline{E}_1$, $\overline{E}_2$ and $\overline{V}$ for the corresponding currents and voltages in Fig. 4.6. The voltage at the fictitious internal bus 1 is then expressed as,

$$\overline{E}_1 = \overline{V} + \overline{Z}_1 \bar{i}_1$$

where $\overline{Z}_1$ is the impedance between bus 0 and bus 1. Keeping in mind that $\overline{V}=V$ is real, the angle δ_1 is obtained as,

$$\delta_1 = \tan^{-1}\left(\frac{\mathrm{Im}\left(\overline{Z}_1 \bar{i}_1\right)}{V + \mathrm{Re}\left(\overline{Z}_1 \bar{i}_1\right)} \right)$$

In [Lerch et al 1991] the term V has been omitted, probably by mistake. If desired, the current measurement can be replaced by measured active and reactive power,

$$\bar{i}_1 = \frac{P_1 + jQ_1}{V}$$

If furthermore the resistive part of the impedance is negligible so that $\overline{Z}_1=\mathrm{j}X_1$, a more convenient expression is obtained,

$$\delta_1 = \tan^{-1}\left(\frac{P_1}{V^2 / X_1 + Q_1} \right) \tag{4.10}$$

δ_2 is obtained from the same expressions by using subscript 2 instead of 1, and the angle difference $\delta=\delta_1-\delta_2$ is computed. The angular frequency of the mode is finally obtained by lead filtering δ.

In [Larsen et al 1995] a CSC damper in a two-area system uses the estimated mode frequency as feedback signal. It is shown that for properly selected $\overline{Z}_1$ and $\overline{Z}_2$ very large damping can be achieved, which means that the feedback signal comes close to the mode coordinate itself. This is remarkable for an estimate based on local measurements. [Larsen et al 1995] further reports that substantial damping can be obtained also for other impedance values, which indicates a certain robustness of the feedback signal.

Except for the work in [Larsen et al 1995] and of [Lerch et al 1991] based on typical two-area systems, the concept of estimating the frequency at an adjacent bus has also been successfully applied to PSS [Kundur 1994, p. 1130]. This case corresponds to the above estimation of δ_1 only. The same technique can also be employed in larger systems, but little can be said about the generic behaviour. While efficient in some cases, it cannot capture mode behaviour in a general system with arbitrary structure of network and modes. In this work estimated mode frequency will therefore only be considered for application in the single mode system used in Chapters 5 and 6.

4.6 Conclusions

The mode observability of bus frequency (or phase angle) is shown to be closely related to the mode controllability of active power. For the simple electro-mechanical power system model full agreement is demonstrated in the geographical variations of these quantities. A direct consequence is that local feedback is preferable since the best place to measure bus frequency is at the bus with highest active power mode controllability. It is also shown that increasing the gain of such a damper from zero will move the eigenvalues of all modes towards better damping. The validity of these results are formally restricted to zero gain. They have, on the other hand, the attractive feature of not being limited to a certain topology or operating point. This is verified by the similarities between the 3D-graphs of bus frequency mode observability in Chapter 3 and active power mode controllability in this chapter. The agreement is, however, not complete which indicates that the model used for the proof is not an entirely valid simplification of the twenty-three machine system at high load.